A&A, 689, A120 (2024)
https://doi.org/10.1051/0004-6361/202451056

Astronomy & Astrophysics

Exploring fluorine chemical evolution in the Galactic disk: The open cluster perspective*

S. Bijavara Seshashayana[1,**], H. Jönsson[1], V. D'Orazi[2,3], N. Sanna[4], G. Andreuzzi[5,6], G. Nandakumar[7], A. Bragaglia[8], D. Romano[8], and E. Spitoni[9]

[1] Materials Science and Applied Mathematics, Malmö University, SE-205 06 Malmö, Sweden
[2] Department of Physics, University of Rome Tor Vergata, Via della Ricerca Scientifica 1, 00133 Rome, Italy
[3] INAF-Osservatorio Astronomico di Padova, Vicolo dell' Osservatorio 5, 35122 Padova, Italy
[4] INAF-Osservatorio Astrofisico di Arcetri, Largo E. Fermi 5, 50125 Firenze, Italy
[5] INAF-Osservatorio Astronomico di Roma, Via Frascati 33, 00178 Monte Porzio Catone, Italy
[6] Fundacíon *Galileo* Galilei – INAF, Rambla José Ana Fernández Pérez 7, 38712 Brena Baja, Tenerife, Spain
[7] Lund Observatory, Division of Astrophysics, Department of Physics, Lund University, 22100 Lund, Sweden
[8] INAF-Osservatorio di Astrofisica e Scienza dello Spazio di Bologna, Via Piero Gobetti 93/3, 40129 Bologna, Italy
[9] INAF-Osservatorio Astronomico di Trieste, Via G. B. Tiepolo 11, 34131 Trieste, Italy

Received 10 June 2024 / Accepted 12 July 2024

ABSTRACT

Context. Open clusters are ideal tools for tracing the abundances of different elements because their stars are expected to have the same age, distance, and metallicity. Therefore, they serve as powerful tracers for investigating the cosmic origins of elements. This paper expands on a recent study by us, in which the element fluorine was studied in seven open clusters; here we add six open clusters and eight field stars.

Aims. The primary objective is to determine the abundance of fluorine (F) to gain insight into its production and evolution. The magnesium (Mg) abundances were derived to categorize the field stars into high and low alpha disk populations. Additionally, cerium (Ce) abundances were determined to better understand the interplay between F and *s*-process elements. Our goal is to analyze the trend of F abundances across the Galactic disk based on metallicity and age. By comparing observational data with Galactic chemical evolution models, the origin of F can be better understood.

Methods. The spectra were obtained from the high-resolution near-infrared GIANO-B instrument at the Telescopio Nazionale *Galileo* (TNG). For the derivation of the stellar parameters and abundances, the Python version of Spectroscopy Made Easy (`PySME`) was used. OH, CN, and CO molecular lines and band heads along with Fe I lines were used to determine the stellar parameters in the *H*-band region. Two HF lines in the *K* band ($\lambda\lambda$ 2.28, and 2.33 μm), three *K*-band Mg I lines ($\lambda\lambda$ 2.10, 2.11, and 2.15 μm), and two Ce II lines in the *H* band ($\lambda\lambda$ 1.66, and 1.71 μm) were used to derive the abundances of F, Mg, and Ce, respectively.

Results. F, Mg, and Ce abundances were derived for 14 stars from 6 OCs, as well as for 8 field stars. The F and Ce abundances were investigated as a function of metallicity, age, and galactocentric distance. We also compared our findings with different Galactic chemical evolution models.

Conclusions. Our results indicate that asymptotic giant branch stars and massive stars, including a subset of fast rotators (whose rotation speed likely increases as metallicity decreases), are necessary to explain the cosmic origin of F. This finding is consistent with and, with the large sample size, reinforces the conclusion of our previous study.

Key words. stars: fundamental parameters – Galaxy: abundances – Galaxy: disk – Galaxy: fundamental parameters – open clusters and associations: general – solar neighborhood

1. Introduction

The study and understanding of the cosmic origins of various elements is of crucial importance for solving the mysteries of the formation and evolution of stars as well as understanding the Galactic chemical evolution (GCE) of these elements. Fluorine (F), an element with an uncertain, –yet interesting and intricate origin, will be discussed in this text. Although F has been suggested to be produced by several sources, its exact origin remains a mystery. Therefore, studying the abundance of F in the solar vicinity and beyond is of great importance. Fluorine possibly originates from one or several of five sources: helium-rich intershells in thermally pulsating asymptotic giant branch (TP-AGB) stars (Busso et al. 1999), the helium-burning cores of massive Wolf-Rayet (W-R) stars with strong stellar winds (Meynet & Arnould 2000), primary F from rotating massive stars (Prantzos et al. 2018), and through the release of neutrino flux in type II supernovae (Woosley & Haxton 1988), – and/or novae (José & Hernanz 1998). The main contributor among these five sources is still uncertain. The study of F has experienced growth in recent years due to the utilization of high-resolution infrared spectrometers, despite the observational challenges: the metal-poor region ([Fe/H] < −0.8 dex), which according to models should be dominated by F production via the ν process and rotating massive stars, has not

* Based on observations made with the Italian Telescopio Nazionale *Galileo* (TNG) operated on the island of La Palma by the Fundación *Galileo* Galilei of the INAF (Istituto Nazionale di Astrofisica) at the Observatorio del Roque de los Muchachos.

** Corresponding author; `shilpa.bijavara-seshashayana@mau.se`

been studied in detail due to the lines of interest becoming very weak.

Nevertheless, based on several observational studies of different environments and comparisons with theoretical models, the five possible contributors have been suggested. Jorissen et al. (1992) studied K and M giants together with AGB stars to determine the abundance of F. The abundance of F for the C-rich AGB stars in this sample was later revised to lower values (Abia et al. 2009, 2010). Still, Jorissen et al. (1992) concluded that AGB stars are the major contributors of Galactic F and that it is produced in the He-burning regions. Carbon-enhanced metal-poor (CEMP) stars were later found to have high F (Schuler et al. 2007; Lucatello et al. 2011). These studies concluded that the high abundances of F in CEMP stars are due to contamination from the previous AGB companions. F has also been detected in helium stars (EHe; Pandey 2006) and R Corona Borealis variable stars (RCrB) (Pandey et al. 2008), where F was found to be overabundant compared to solar values. Since these objects are thought to be in the AGB phase, this could be a potential source of F. Recio-Blanco et al. (2012) studied F in dwarf stars in the solar neighborhood, D'Orazi et al. (2013) in the globular cluster M 22, Werner et al. (2005) in a hot post-AGB star, Zhang & Liu (2005) and in planetary nebulae, and all concluded that AGB stars are the major contributors. While there is therefore evidence that AGB stars produce F, others of the five mentioned sources may also be involved, leading to some competing notions. Cunha et al. (2003) analyzed F abundances in the Large Magellanic Cloud and found that AGB stars did not in fact play a predominant part. An investigation of the Milky Way bulge concluded that F is formed from a mixture of AGB and W-R stars (Cunha et al. 2008). Theoretical works by Spitoni et al. (2018) and Grisoni et al. (2020) suggest that AGB stars are one possible source, but not necessarily the dominant one. Many EHe stars exhibit overabundances of F in a recent study by Bhowmick et al. (2020). When correlated with C, O, and Ne, it was suggested that they were produced by He and CO white dwarf mergers, as modeled by Menon et al. (2013, 2019), and Lauer et al. (2019). Although various studies with different objects conclude that AGB stars likely are the essential driving progenitor of the GCE of F, W-R stars and ν processes remain viable sources. The plausible astrophysical sites have been included as potential sources in various GCE models (Timmes et al. 1995; Kobayashi et al. 2011a,b; Prantzos et al. 2018; Spitoni et al. 2018; Grisoni et al. 2020). Furthermore, many observational studies have suggested multiple cosmic sources for F, for example, Jönsson et al. (2014a,b, 2017), Pilachowski & Pace (2015), Guerço et al. (2019), and Ryde et al. (2020).

The cosmic origin of F is challenging to discern and track due to the absence of robust atomic F lines in the optical or infrared portions of the electromagnetic spectrum. The highly ionized and excited atomic lines of F V and F VI, seen between 1050 and 1150 Å, are only observed in hot stars (85 000–150 000 K) in the far-ultraviolet (Werner et al. 2005). The F I at 6800–7800 Å in optical spectra of stars has only been used to study EHe and RCrB stars, which have high temperatures (>6500 K) (Pandey 2006; Pandey et al. 2008). For cool stars, the only lines available are infrared lines from the HF molecule. Its dissociation energy (D_0) is 5.87 eV (Sauval & Tatum 1984), which is rather low, making the lines weak for $T_{\rm eff} > 4500$ K, when the molecule becomes dissociated. Combined with the fact that the abundance of F in stars is generally already low, this makes it difficult to trace the Galactic F trend.

All the abovementioned observational studies and models concentrated on field stars. However, open clusters (OCs) offer valuable insight into abundances, stellar chemistry, and the evolution of the Galaxy, as they contain stars with comparable ages, metallicities, and galactocentric radii ($R_{\rm gc}$). For this reason, they are known as "ideal laboratories" for testing stellar and Galactic formation and evolution models (Friel 1995; Lada & Lada 2003). Over the past few decades, OCs have been the subject of several studies (see, e.g., Janes 1979; Bragaglia et al. 2008; Friel et al. 2010; Carrera & Pancino 2011; Carbajo-Hijarrubia et al. 2024). More recently, clusters have also been a subject of study in surveys, for instance, the *Gaia*–European Southern Observatory (*Gaia*–ESO; Magrini et al. 2017, 2023; Romano et al. 2021) survey, the GALactic Archaeology with HERMES (GALAH; Spina et al. 2022) survey, and the Apache Point Observatory Galactic Evolution Experiment (APOGEE; Myers et al. 2022). However, no current or planned survey will be able to determine F abundances since none cover the K band. Smaller-scale works that map the F abundances together with the metallicity ([Fe/H]), age, and $R_{\rm gc}$ (like this paper) will therefore be an important source of information for understanding the evolution of Galactic F. The correlation between F abundances and age and/or $R_{\rm gc}$ in OCs has not yet been extensively studied. Nault & Pilachowski (2013) used the PHOENIX spectrometer to determine the abundance of F in the Hyades, NGC 752, and M 67 OCs and concluded that multiple sources may contribute to the F abundance in the disk of our Galaxy and that it is unlikely that AGB is the dominant source. A study by Maiorca et al. (2014) of the OC NGC 6404, using CRIRES at the Very Large Telescope emphasized the significance of the contribution of low-mass AGB stars. Holanda et al. (2024) determined the abundances of 20 elements, including F, in the OC NGC 2345. The stars studied in the cluster show a consistent ratio of F to Fe, indicating a subsolar abundance of F. Because of all the challenges and constraints mentioned above, more theoretical and observational evidence is needed to determine the cosmic budget of F, which makes it both an interesting and active field of research.

In our recent study (Seshashayana et al. 2024) we presented the F and Ce abundances of seven OCs. The abundances were presented in relation to metallicities, ages, and $R_{\rm gc}$, –and compared with GCE models. In the study, we found a solar pattern in [F/Fe] without any secondary behavior for stars with solar or super-solar metallicity, with the notable exception of NGC 6791. A comparison between the F abundances and GCE models led us to the conclusion that both AGB stars and massive stars, including a fraction of fast rotators that increases with decreasing metallicity, are necessary to explain the cosmic origin of F. The present study builds on and extends this previous work by determining F and Ce abundances for six additional OCs: NGC 6939, NGC 7762, NGC 7142, Collinder 110, Berkeley 32, and NGC 2420, thus extending the already largest homogeneous database for the determination of F in OCs. The objective of selecting these OCs was to increase the number of intermediate-age and old clusters in the database and to improve the coverage in $R_{\rm gc}$. This will facilitate a more comprehensive study of the history of F enrichment in both space and time. In these OCs, there are giants that are sufficiently cool to permit the measurement of F. In addition, we observed six field stars, –that were mainly targeted because they have well-determined stellar parameters and hence serve as a test case for the method used to derive stellar parameters. Furthermore, the stars were sufficiently cool to allow the detection of F.

Table 1. Basic information for our program stars, including the eight field stars, and their spectra.

Stellar cluster	Star	*Gaia* DR3 ID	RA (deg)	Dec (deg)	G (mag)	S/N H band	S/N K band
NGC 6939	NGC 6939_1	2194725337620737792	307.690027985254	60.60090033682878	10.34	249	216
Age = 1.70 Gyr	NGC 6939_2	2194824018782231296	307.751916928197	60.81436876801729	11.12	224	199
R_{gc} = 8.70 kpc	NGC 6939_3	2194726471490897024	307.518549581646	60.55418772365226	11.19	148	132
	NGC 6939_4	2194713139912733056	307.918942123322	60.61892205660228	11.32	166	145
NGC 2420	NGC 2420_1	865399939794984320	114.56276636	21.5830497562	11.14	198	172
Age = 1.74 Gyr							
R_{gc} = 10.68 kpc							
Collinder 110	Cr 110_2	3126738188653591168	99.805185271	2.0493381003	11.05	230	194
Age = 1.82 Gyr	Cr 110_3	3126749767885447552	99.738812533	2.05903237577	10.98	254	230
R_{gc} = 10.29 kpc	Cr 110_4	3126754234651093888	99.686343516	2.14405637405	10.19	390	326
NGC 7762	NGC 7762_1	2210930249228141056	357.800686711477	67.94158562607588	10.41	262	230
Age = 2.04 Gyr							
R_{gc} = 8.78 kpc							
NGC 7142	NGC 7142_1	2217941937956979840	326.260545852642	65.76114212449832	11.26	186	162
Age = 3.09 Gyr	NGC 7142_2	2217944274419272960	326.705463196390	65.76928923282846	11.71	171	151
R_{gc} = 9.25 kpc	NGC 7142_3	2217943587224390912	326.291673041744	65.85459299930302	12.01	132	112
Berkeley 32	Be 32_1	3129900070557039488	104.51412308	6.44718036949	11.66	254	230
Age = 4.90 Gyr	Be 32_2	3129898833606459904	104.51319996	6.40616048404	11.80	148	115
R_{gc} = 11.14 kpc							
	HIP 3786	2556759229189045632	12.170968944689	7.5848586637986	3.84	438	395
	HIP 4147	2535891460567764224	13.252085422292	−1.1443296982576	4.12	493	383
	KIC 5182451	2101176414429414528	290.400321483165	40.3197644483823	10.54	87	78
	KIC 8414116	2106673762107078656	284.096587350876	44.4797275017186	10.09	219	190
	KIC 8427166	2126971850569328128	290.462597612610	44.4461778834982	10.69	185	169
	KIC 12252278	2133370527203207040	287.902989291060	50.9613014077372	10.69	142	123
	KIC 11076239	2131204145699718528	287.619303757366	48.6328776694531	10.25	136	120
	KIC 10801138	2128855726303447296	293.429473531675	48.1947937842640	10.00	202	176

Notes. The ages and R_{gc} for the OCs are from Cantat-Gaudin et al. (2020). The header of each file containing the spectrum information was employed to obtain the signal-to-noise ratios (S/N). This was achieved by utilizing the value for order 48 as a reference for the H band and order 33 for the K band.

2. Observations

The Telescopio Nazionale *Galileo* (TNG), with a diameter of 3.6 m, was used to observe our sample of cluster and field stars (program: A47TAC_6) in March and August 2023, using GIARPS (GIANO-B + HARPS-N mode). The instrument configuration allows us to simultaneously observe using the High Accuracy Radial Velocity Planet Searcher for the Northern hemisphere (HARPS-N) spectrograph (R = 115 000, $\lambda\lambda$ = 3800−6900 Å, Cosentino et al. 2014) and GIANO-B near-infrared (NIR) spectrograph (R = 50 000, $\lambda\lambda$ = 0.97−2.5 µm; Oliva et al. 2012a,b; Origlia et al. 2014). However, since we focused on the NIR part of the spectra, the observing times were calculated using the GIANO-B Exposure Time Calculator, to ensure a S/N of around 150 in the K band when observing at an airmass of 1.5 and a typical seeing condition of 1.2 arcsec. During observations, GIANO-B spectra were collected by nodding the star along the slit, with the target alternatively positioned at 1/4 (position A) and 3/4 (position B) of the slit length for the same amount of time, with single AB nodding exposures of 300 seconds. Fast-rotating hot stars were observed for telluric correction. These stars were observed twice per night at different airmasses. The spectra were processed with the GOFIO reduction software (Rainer et al. 2018), and telluric contamination was eliminated using the standard Image Reduction and Analysis Facility (IRAF) technique described, for example, in Ryde et al. (2019). The basic information regarding all objects can be found in Table 1.

3. Analysis

The observed spectra were analyzed using the Python version of Spectroscopy Made Easy (`PySME`) (Piskunov & Valenti 2017; Valenti & Piskunov 1996; Wehrhahn et al. 2023), – following the methodology employed in our previous investigation (Seshashayana et al. 2024). We used one-dimensional spherical MARCS models (Gustafsson et al. 2008) and line lists retrieved from VALD3 (Kupka et al. 1999, 2000; Piskunov et al. 1995). `PySME` has support for the use of nonlocal thermodynamic equilibrium (non-LTE) departure coefficient grids, which greatly improves the accuracy in the synthesis of many lines (Amarsi et al. 2016, 2018). For the present work, non-LTE synthesis has been used for Mg and Fe lines.

The HF lines used here are R9 at λ_{air} = 23358.329 Å and R16 at λ_{air} = 27778.249 Å. Jönsson et al. (2014a) provides a comprehensive review of the vibrational-rotational K-band HF lines. The Ce II lines are at 16595.180 Å and 17058.880 Å (Corliss 1973). The log gf was determined astrophysically for Ce II lines, where a reference abundance is set for an element, and the synthetic spectra are fitted by varying the log gf value for an observed spectrum of the Sun or another reference star, in this case Arcturus (Cunha et al. 2017). These values were subsequently adjusted slightly by Montelius et al. (2022) to be consistent with abundances derived for the same stars in the solar neighborhood using optical spectra. These values by Montelius et al. (2022) were adapted in our study. The

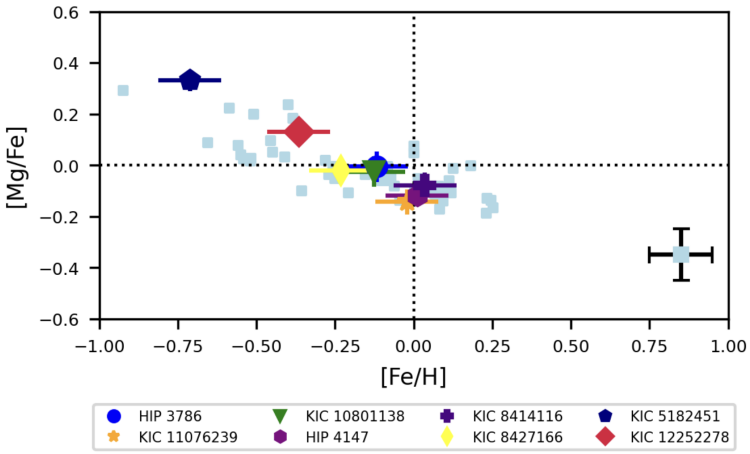

Fig. 1. [Mg/Fe] versus [Fe/H]. The field stars are plotted for Mg to identify and categorize which are high and low alpha disk stars. The light blue squares are taken from Nandakumar et al. (2023a). Representative uncertainties are shown in the bottom-right corner.

Table 2. Lines used to determine magnesium, fluorine, and cerium abundances.

Species	λ_{air} (Å)	log (gf)	E_{low} (eV)	Reference
HF	22778.249	−3.969	0.674	Jönsson et al. (2014a)
HF	23358.329	−3.962	0.227	Jönsson et al. (2014a)
Mg I	21059.757	−0.384	6.779	Civiš et al. (2013)
Mg I	21060.896	−1.587	6.779	Civiš et al. (2013)
Mg I	21060.896	−0.407	6.779	Civiš et al. (2013)
Mg I	21458.962	−1.319	6.516	Nandakumar et al. (2023a)
Ce II	16595.180	−2.114	0.122	Montelius et al. (2022)
Ce II	17058.880	−1.425	0.318	Montelius et al. (2022)

lines used to determine Mg abundances are from the K-band multiplet lines at 21059.76 Å, 21060.89 Å, and 21458.87 Å (this line has a log gf value with an accuracy of grade B+ in the NIST database). The Mg lines available in our spectra at 15740.70 Åand 15748.89 Å are excluded from consideration due to saturation and a pronounced correlation with v_{mic} (Nandakumar et al. 2023a).

3.1. Stellar parameters

The stellar parameters, such as T_{eff}, log g, [Fe/H], and microturbulence (v_{mic}), are crucial for the analysis of observed spectra. However, analyzing cool stars ($T_{eff} \lesssim 4500$ K) is difficult because many lines become saturated. The method that we employed for our objects is the one of Nandakumar et al. (2023a), which has been developed especially for the cooler stars and was also used in our previous analysis (Seshashayana et al. 2024). In this iterative method, all stellar parameters except for log g are determined from the H-band spectra using `PySME`, while log g is found from isochrones. The fitting procedure is done using a selection of T_{eff}-sensitive OH lines and metallicity-sensitive Fe I lines. Since abundances of C, N, and O are coupled via molecular equilibria, we set as free parameters also C and N, using lines from CN and CO. These features serve to constrain the abundances of C and N, as well as aid in fitting the CO and CN blends in the observed spectra. However, the OH lines are sensitive not only to T_{eff} but also to O abundance. Therefore, the method needs to have a fixed O abundance to constrain the T_{eff} from the OH lines. To do this, Nandakumar et al. (2023a) used functional forms of trends based on the Amarsi et al. (2019) three-dimensional non-LTE (3D NLTE) O abundances to calculate [O/Fe] for stars in both the high and low alpha disks for all metallicities. This would make [O/Fe] 0.0 for a solar-metallicity low-alpha star and 0.15 for a high-alpha star. After the fit, log g is set from the Yonsei-Yale isochrones (Demarque et al. 2004). `PySME` is then once again used to determine the best fit for the selected spectral lines. The values of T_{eff}, [Fe/H], v_{mic}, C, and N abundances from the previous cycle will be utilized as new starting values for the subsequent iteration. This process continues until the deviation from the previous cycle is close to zero. As our sample includes field stars, it is necessary to determine whether these stars belong to the high or low alpha disk to set the O to a reasonable value. To accomplish this, we determined the Mg abundances. If the stars belong to the high-alpha disk, we recalculated the stellar parameters using the O abundances appropriate for a high-alpha disk star, – (see Figure 1). Nandakumar et al. (2023a) estimated an expected error of ±100 K for T_{eff}, ±0.2 dex for log g, ±0.1 dex for [Fe/H], ±0.1 km s^{-1} for v_{mic}, ±0.1 dex for [C/Fe], and ±0.1 dex for [N/Fe] using this method.

3.2. Abundances of F, Mg, and Ce

The abundances of F, Mg, and Ce were derived using the line list information provided in Table 2. From the [Mg/Fe] versus [Fe/H] trend in Fig. 1, two Kepler Input Catalog (KIC) stars (KIC 5182451 and KIC 12252278) were identified as belonging to the high alpha disk population. For these two stars, the O abundance was set following the high alpha disk trend when determining the stellar parameters. The remaining field stars and all stars belonging to the OCs instead were set following the low alpha disk trend. The [Mg/Fe] values obtained for all the stars in the field

Table 3. Stellar parameters and abundances for the OC stars.

Star	$T_{\rm eff}$ (K)	$\log g$ (dex)	[Fe/H] (dex)	$v_{\rm mic}$ (km s^{-1})	$v_{\rm mac}$ (km s^{-1})	[C/Fe] (dex)	[N/Fe] (dex)	[O/Fe] (dex)	[Mg/Fe] (dex)	[F/Fe] (dex)	[Ce/Fe] (dex)
NGC 6939_1	3980	1.53	0.00	1.67	8.15	−0.17	0.23	−0.04	−0.12 ± 0.04	−0.13 ± 0.12	0.06 ± 0.08
NGC 6939_2	4106	1.77	0.00	1.53	8.58	−0.16	0.23	−0.04	−0.14 ± 0.05	−0.17 ± 0.14	0.19 ± 0.10
NGC 6939_3	4285	2.10	−0.03	1.68	8.13	−0.13	0.18	−0.03	−0.08 ± 0.04	−0.29 ± 0.13	0.12 ± 0.07
NGC 6939_4	4297	2.12	−0.02	1.56	7.13	−0.14	0.26	−0.03	−0.14 ± 0.06	−0.18 ± 0.14	0.18 ± 0.08
NGC 2420_1	4083	1.61	−0.16	1.60	7.03	−0.21	0.22	0.02	−0.05 ± 0.04	−0.16 ± 0.16	0.30 ± 0.09
Cr 110_2	4026	1.56	−0.08	1.51	7.78	−0.17	0.19	−0.01	−0.08 ± 0.06	−0.33 ± 0.15	0.23 ± 0.09
Cr 110_3	4005	1.48	−0.13	1.62	8.54	−0.12	0.19	0.01	−0.08 ± 0.04	−0.23 ± 0.15	0.17 ± 0.07
Cr 110_4	3701	0.95	−0.08	1.90	7.87	−0.16	0.28	−0.01	−0.07 ± 0.05	−0.25 ± 0.12	0.05 ± 0.07
NGC 7762_1	4201	1.93	−0.03	1.59	7.67	−0.14	0.24	−0.03	−0.15 ± 0.05	−0.15 ± 0.16	0.25 ± 0.06
NGC 7142_1	3942	1.49	0.05	1.75	8.95	−0.13	0.21	−0.06	−0.03 ± 0.04	−0.19 ± 0.12	−0.10 ± 0.06
NGC 7142_2	4072	1.72	0.04	1.66	7.62	−0.16	0.22	−0.05	−0.11 ± 0.04	−0.27 ± 0.13	−0.06 ± 0.09
NGC 7142_3	4130	1.83	0.03	1.45	8.06	−0.15	0.30	−0.05	−0.16 ± 0.03	−0.24 ± 0.16	0.02 ± 0.10
Be 32_1	4007	1.48	−0.14	1.61	6.67	−0.13	0.19	0.01	−0.09 ± 0.06	−0.23 ± 0.17	0.19 ± 0.09
Be 32_2	4132	1.60	−0.31	1.50	6.52	−0.15	0.23	0.07	−0.08 ± 0.05	−0.07±0.20	0.09 ± 0.08

Notes. Abundance ratios are scaled to the solar values of $A(C)_\odot = 8.46$, $A(N)_\odot = 7.83$, $A(O)_\odot = 8.69$, $A(Mg)_\odot = 7.55$, $A(F)_\odot = 4.40$, $A(Fe)_\odot = 7.46$, and $A(Ce)_\odot = 1.58$ (Asplund et al. 2021). Typical uncertainties of our derived stellar parameters are ±100 K in $T_{\rm eff}$, ±0.2 dex in $\log g$, ±0.1 dex in [Fe/H], ±0.1 km s^{-1} in $v_{\rm mic}$, ±0.1 dex in [C/Fe], and ±0.1 dex in [N/Fe]. The values given here for $v_{\rm mac}$ are derived from the *H* band.

Table 4. Stellar parameters and abundances for all the *Kepler* field stars.

Star	$T_{\rm eff}$ (K)	$\log g$ (dex)	$\log g_{\rm A}$ (dex)	[Fe/H] (dex)	$v_{\rm mic}$ (km s^{-1})	$v_{\rm mac}$ (km s^{-1})	[C/Fe] (dex)	[N/Fe] (dex)	[O/Fe] (dex)	[Mg/Fe] (dex)	[F/Fe] (dex)	[Ce/Fe] (dex)
KIC 5182451	3776	0.73	0.64	−0.67	1.96	6.73	0.05	0.06	0.43	0.33 ± 0.04	−0.19 ± 0.12	−0.12 ± 0.07
KIC 8414116	3991	1.45	1.44	0.05	1.48	8.23	−0.16	0.12	−0.06	−0.08 ± 0.05	−0.13 ± 0.11	−0.14 ± 0.08
KIC 8427166	3556	0.63	0.58	−0.21	1.77	8.84	−0.13	0.06	0.03	−0.02 ± 0.05	0.11 ± 0.09	−0.15 ± 0.10
KIC 10801138	3997	1.46	1.33	−0.19	1.57	7.96	−0.16	0.23	0.00	−0.03 ± 0.06	−0.09 ± 0.14	0.04 ± 0.08
KIC 11076239	4018	1.60	1.42	0.00	1.63	7.77	−0.15	0.17	−0.05	−0.14 ± 0.05	−0.03 ± 0.16	−0.08 ± 0.07
KIC 12252278	4021	1.35	1.29	−0.35	1.50	8.69	−0.03	0.14	0.28	0.13 ± 0.05	−0.30 ± 0.13	−0.10 ± 0.09

Notes. Our derived $\log g$ values have been compared with asteroseismic $\log g$ values that are represented as $\log g_{\rm A}$. The uncertainties of $\log g_{\rm A}$ are all within 0.01 dex. For solar reference values, uncertainties, and $v_{\rm mac}$ of our values, see the caption of Table 3.

Table 5. Stellar parameters and abundances for the field stars with measured angular diameters from Baines et al. (2021) that is represented as $T_{\rm teff,A}$.

Star	$T_{\rm eff}$ (K)	$T_{\rm teff,A}$ (K)	$\log g$ (dex)	[Fe/H] (dex)	$v_{\rm mic}$ (km s^{-1})	$v_{\rm mac}$ (km s^{-1})	[C/Fe] (dex)	[N/Fe] (dex)	[O/Fe] (dex)	[Mg/Fe] (dex)	[F/Fe] (dex)	[Ce/Fe] (dex)
HIP 3786	3927	3868 ± 35	1.36	−0.11	1.61	6.75	−0.11	0.16	−0.01	−0.01 ± 0.06	−0.08± 0.12	−0.17 ± 0.10
HIP 4147	3883	3724 ± 35	1.36	0.02	1.60	8.57	−0.22	0.16	−0.05	−0.12 ± 0.04	−0.19± 0.12	0.24 ± 0.08

Notes. For solar reference values, uncertainties, and the $v_{\rm mac}$ of our values, see the caption of Table 3.

Table 6. Averaged abundance values of the six clusters.

Stellar cluster	Age (Gyr)	$R_{\rm GC}$ (kpc)	[Fe/H] (dex)	[Mg/Fe] (dex)	[Mg/H] (dex)	[F/Fe] (dex)	[F/H] (dex)	[Ce/Fe] (dex)	[Ce/H] (dex)
NGC 6939	1.70	8.70	−0.01 ± 0.01	−0.12 ± 0.02	−0.13 ± 0.02	−0.19 ± 0.04	−0.21 ± 0.04	0.14 ± 0.04	0.12 ± 0.05
NGC 2420	1.74	10.68	−0.16 ± 0.04	−0.05 ± 0.03	−0.21 ± 0.06	−0.16 ± 0.04	−0.31 ± 0.03	0.30 ± 0.04	0.14 ± 0.07
Collinder 110	1.82	10.29	−0.10 ± 0.04	−0.08 ± 0.01	−0.17 ± 0.03	−0.27 ± 0.02	−0.40 ± 0.01	0.14 ± 0.05	0.04 ± 0.08
NGC 7762	2.04	8.78	−0.03 ± 0.04	−0.15 ± 0.03	−0.18 ± 0.06	−0.15 ± 0.04	−0.18 ± 0.03	0.16 ± 0.04	0.13 ± 0.07
NGC 7142	3.09	9.25	0.04 ± 0.01	−0.10 ± 0.07	−0.06 ± 0.07	−0.23 ± 0.03	−0.19 ± 0.01	−0.05 ± 0.04	−0.01 ± 0.03
Berkeley 32	4.90	11.14	−0.22 ± 0.08	−0.09 ± 0.01	−0.31 ± 0.12	−0.15 ± 0.08	−0.37 ± 0.04	−0.04 ± 0.05	−0.26 ± 0.14

Notes. The uncertainties mentioned above are computed from the root mean square deviation from the mean of the values obtained for individual stars within the cluster, except for NGC 7762 and NGC 2420, where we have only one star in our sample. For these clusters, the reported uncertainties are instead representative measures that are based on the average uncertainties of the other clusters.

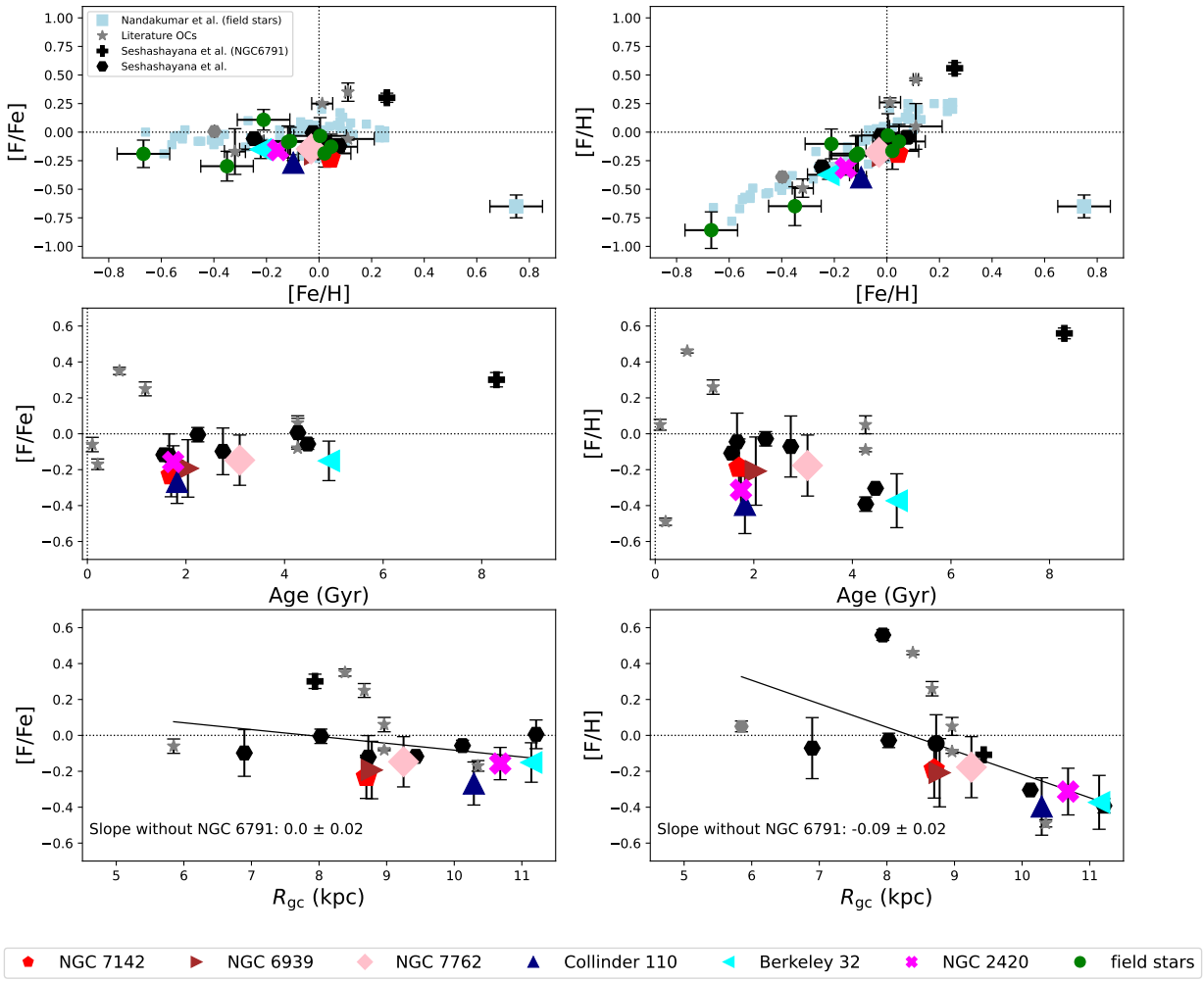

Fig. 2. Left: Relationship between [F/Fe] and [Fe/H], age, and R_{gc}. Right: Same but for [F/H]. Field stars from Nandakumar et al. (2023b) are depicted as light blue squares. A representative error bar for the data from Nandakumar et al. (2023b) is shown in the bottom-right corner in the first row of panels. The black hexagons are the OCs studied in our previous paper, Seshashayana et al. (2024). We also plot values for five OCs as light gray stars, namely Hyades, NGC 752, and M 67 from Nault & Pilachowski (2013), another estimate of M 67 and another cluster, NGC 6404, from Maiorca et al. (2014), and NGC 2345 from Holanda et al. (2024). The slopes were obtained via a fit to all strictly similarly analyzed OCs from this and our previous work, excluding the outlier NGC 6791 (see Seshashayana et al. 2024, for a discussion).

are in agreement with the corresponding trend obtained for the stars in the solar neighborhood by Nandakumar et al. (2023a). The values of [Mg/Fe], as well as the other determined abundances, are given in Tables 3–5.

To estimate the uncertainties of the derived abundances in the individual stars, we, as in our previous study, also redetermined the abundances using 100 different values of $T_{\rm eff}$, $\log g$, [Fe/H], and $v_{\rm mic}$ using a random normal distribution around the parameters we obtained. The evaluation was based on the methodological uncertainty estimates by Nandakumar et al. (2023a). Hence, each spectrum was analyzed 100 times using 100 different sets of stellar parameters, which yielded 100 different F, Mg, and Ce abundance values. The abundance uncertainties for the individual stars in Tables 3–5 are given as the median absolute deviation of the individual abundance uncertainties for each star.

Furthermore, just as in our previous analysis, two $v_{\rm mac}$ determinations were performed. A smaller $v_{\rm mac}$ has been chosen from the H band lines and is used for the determination of Ce abundances from the H-band, and a slightly larger value was set for the K-band HF lines. The reason for this is to account for the slight variation in the instrument resolution with wavelength.

4. Results and discussion

The main results are presented in Tables 3–6 and illustrated in Figures 2–4. The relationships between [F/Fe], [Ce/Fe], [F/H], and [Ce/H] with age and R_{gc} were investigated only for our OCs. For field stars, only the relationship between [F/Fe], [Ce/Fe], [F/H], and [Ce/H] with [Fe/H] was explored. The results are compared with GCE models that implement different stellar sources of F in Figure 4.

4.1. Comparison of our stars' parameters with literature values

Six stars were taken from the *Kepler* database, and they all have asteroseismic $\log g$-values in the APOGEE and Kepler Asteroseismology Science Consortium (APOKASC-3) catalog (private communication, Pinsonneault et al., in prep.), that can be used to test the performance of our iterative method for deriving $\log g$ using spectra and isochrones. The agreement is generally very good, –see Table 4.

The two HIP stars have $T_{\rm eff}$ determined from angular diameter measurements (Baines et al. 2021), which can be used to

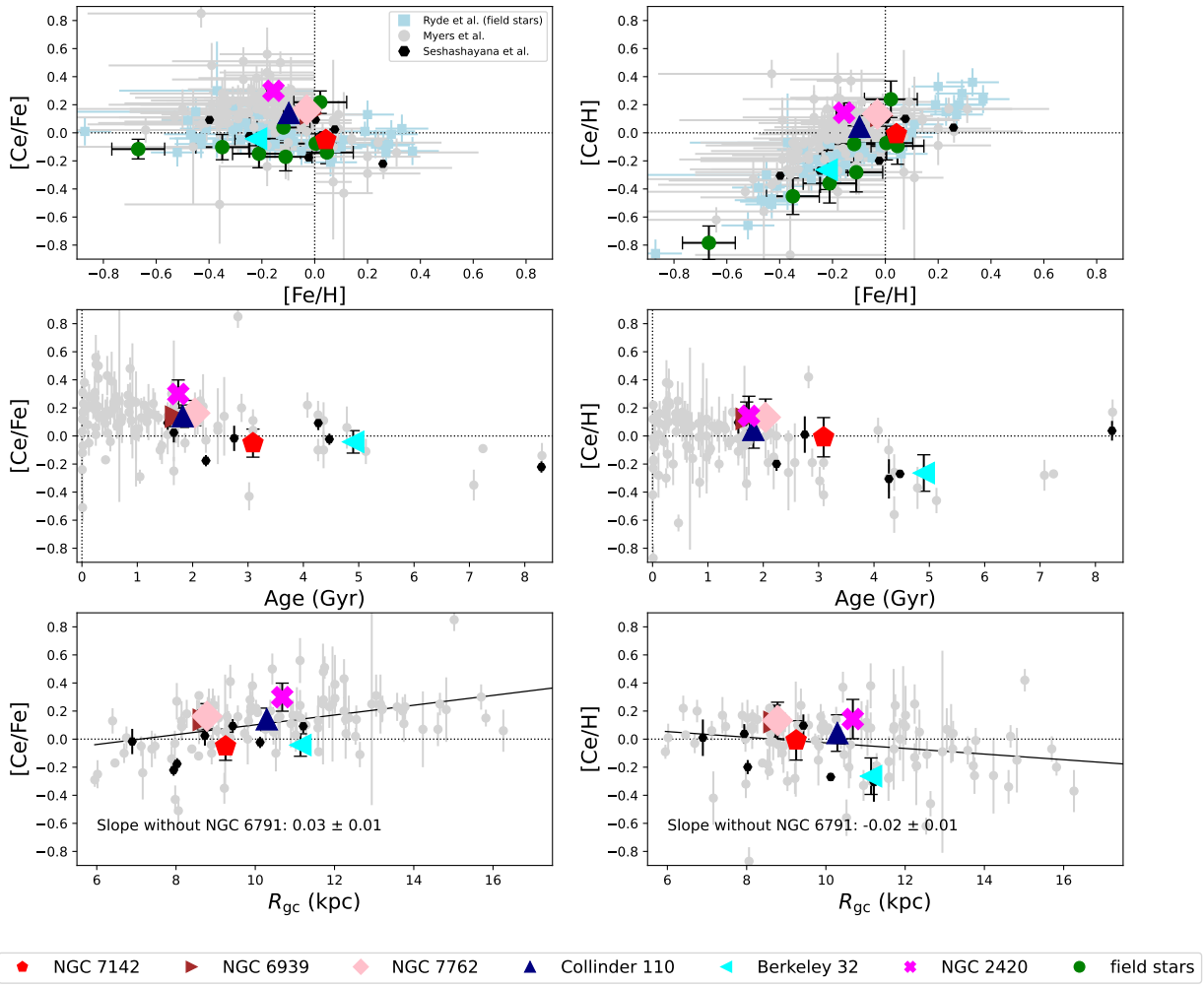

Fig. 3. Relationship between [Ce/Fe] and [Fe/H], age, and R_{gc} (left) and [Ce/H] as a function of [Fe/H], age, and R_{gc} (right). The black hexagons are the OCs studied in our previous paper, Seshashayana et al. (2024). Data for field stars taken from Ryde et al. (2020) are shown as light blue dots. The clusters taken from Myers et al. (2022) are shown as light gray squares. The slopes were obtained via a fit to all strictly similarly analyzed OCs from this and our previous work, excluding the outlier NGC 6791 (see Seshashayana et al. 2024, for a discussion).

assess our ability to correctly derive T_{eff}. The resulting values are well within the error ranges (see Table 5).

The cluster metallicities we determined are compared with a few literature values in Table 7. The table presents our [Fe/H] values, the corresponding literature values, and the respective literature references for all six clusters. The resultant metallicities are well within the range of error in comparison to previous literature values.

4.2. F and Ce abundances

In Figure 2, the metallicity is plotted with [F/Fe] and [F/H] for our OCs and field stars. The results are presented in combination with the field stars from Nandakumar et al. (2023b) in the upper panels. Our results are also plotted with the literature OCs for [Fe/H], age, and R_{gc} (see the upper, middle, and lower panels). Additionally, a comparison is presented between the current study and our previous results (seven OCs that we had previously studied; see Seshashayana et al. 2024). The data points align with the literature on OCs and field stars. At super-solar metallicities, F exhibits a secondary behavior in Ryde et al. (2020) and Guerço et al. (2022), which is not present in Nandakumar et al. (2023b). Our results also support those of Nandakumar et al. (2023b), as the stronger and possibly saturated/blended HF R9 line, which shows temperature-dependent trends, is found to have high uncertainty, especially in cooler and metal-rich giant stars (for a detailed explanation, see Nandakumar et al. 2023b). The middle and lower panels are compared with literature OCs that have been previously analyzed for F. Since the age and R_{gc} for field stars are less reliable than for OCs, these panels only contain our clusters and not field stars. Hyades, NGC 752, M 67 from Nault & Pilachowski (2013), NGC 2345 from Holanda et al. (2024), and finally M 67 (again) and NGC 6404 from Maiorca et al. (2014) comprises all the OCs that have been employed thus far to investigate F, disregarding our previous paper. Our combined dataset from the previous and this paper, together with NGC 2345, shows a uniform flat trend between about 200 Myr and 6 Gyr, except for NGC 6791, which shows a high [F/Fe] ratio (see Seshashayana et al. 2024 for more details). For the clusters analyzed by us, there is a downward trend when [F/H] is plotted against age and R_{gc}, which is in agreement with standard chemical evolution and the presence of the Galactic metallicity gradient. However, the literature OCs NGC 752, Hyades, and NGC 2345 deviate significantly from the data analyzed by us, rendering it inadvisable to draw any inferences when plotted

Table 7. Comparison of our metallicity values with those found in the literature.

Stellar cluster	[Fe/H] determined in this article (dex)	Literature [Fe/H] value (dex)	Literature reference
NGC 6939	−0.01 ± 0.01	−0.19 ± 0.1	Friel et al. (2002)
		0.00 ± 0.1	Jacobson et al. (2007)
		−0.02 ± 0.15	Overbeek et al. (2016)
NGC 7142	0.04 ± 0.01	−0.10 ± 0.1	Friel et al. (2002)
		0.08 ± 0.06	Jacobson et al. (2007)
NGC 7762	−0.03 ± 0.04	0.04 ± 0.12	Carraro et al. (2016)
Berkeley 32	−0.22 ± 0.08	−0.29 ± 0.1	Sestito et al. (2006)
		−0.21 ± 0.01	Friel et al. (2010)
		−0.26 ± 0.06	Overbeek et al. (2016)
		−0.31 ± 0.2	Zhong et al. (2020)
		−0.38 ± 0.06	Spina et al. (2021)
		−0.31 ± 0.06	Randich et al. (2022)
		−0.37 ± 0.2	Fu et al. (2022)
Collinder 110	−0.10 ± 0.04	0.04 ± 0.05	Pancino et al. (2010)
		−0.1 ± 0.04	Randich et al. (2022)
NGC 2420	−0.16 ± 0.04	−0.20 ± 0.06	Jacobson et al. (2011)
		−0.05 ± 0.05	Pancino et al. (2017)
		−0.12 ± 0.02	Donor et al. (2018)
		−0.12 ± 0.03	Carrera et al. (2019)
		−0.19 ± 0.03	Spina et al. (2021)
		−0.20 ± 0.04	Myers et al. (2022)
		−0.15 ± 0.02	Randich et al. (2022)

Notes. Each value is referenced.

with our data. Lastly, when [F/Fe] is plotted against age, a flat trend is seen. The OCs from the current analysis follow the trend of our previous OCs. The slope for [F/Fe] versus R_{gc} without NGC 6791 is 0.00 ± 0.02 dex/kpc. The value from the previous analysis in Seshashayana et al. (2024) is 0.01 ± 0.02 dex/kpc. In our current study, when we calculate the slope for [F/H] versus R_{gc} for all of our clusters except NGC 6791, we find a value of −0.09 ± 0.02 dex/kpc. The slope from our previous analysis for [F/H] versus R_{gc} (see Seshashayana et al. 2024) is −0.09 ± 0.03 dex/kpc. The slope value provided by the current sample of stars compared to our previous results indicates that the data are consistent across a wider range of stars, providing a more comprehensive and robust understanding of the behavior of F.

The same was done for Ce, where [Ce/Fe] and [Ce/H] were compared with [Fe/H], age, and R_{gc}. Figure 3 shows the behavior of Ce for our clusters. We compared with literature OCs from Myers et al. (2022) and some field stars from Ryde et al. (2020). The OCs from Myers et al. (2022) are from the APOGEE survey (DR17, Abdurro'uf et al. 2022), and include 150 OCs. However, we extracted clusters with available data on ages, distances, and [Ce/Fe] values, resulting in a subsample of 104 OCs for head-to-head comparison with our results. Our current analysis shares one cluster, NGC 2420, and from our previous analysis, four clusters (NGC 6791, NGC 6819, Trumpler 5, and NGC 7789) with Myers et al. (2022). The upper panels show that our obtained values are in good general agreement with those reported by both Myers et al. (2022) and Ryde et al. (2020). From our current analysis, the [Ce/Fe] value of NGC 2420 is 0.30 ± 0.09 and from Myers et al. (2022) it is 0.16 ± 0.14, which makes our value higher, although within the observational uncertainty. For [Ce/Fe] relative to age, there is a flat trend, while for R_{gc} there is an increasing trend. For [Ce/H] relative to age and R_{gc}, there is a decreasing trend. This suggests that younger clusters tend to have higher Ce abundance compared to their older counterparts. This finding is in line with previous studies on s-process elements in OCs, indicating a rising trend in younger clusters (D'Orazi & Randich 2009; Maiorca et al. 2011; Yong et al. 2012; Mishenina et al. 2015; D'Orazi et al. 2022; Magrini et al. 2023). The increasing trend of [Ce/Fe] with R_{gc} confirms previous findings on OCs in for example, *Gaia*-ESO, such as those by Viscasillas Vázquez et al. (2022) and Magrini et al. (2023). The calculated slope for all our clusters is given in Fig. 3 and the value is 0.03 ± 0.01 dex/kpc (without NGC 6791); this is in good agreement with the findings of Myers et al. (2022) who found 0.02 ± 0.01 dex/kpc. According to our analysis (and excluding NGC 6791), the value for [Ce/H] versus R_{gc} is −0.02 ± 0.01 dex/kpc. The value from our previous results (see Seshashayana et al. 2024) for [Ce/Fe] versus R_{gc} is 0.03 ± 0.03 dex/kpc and [Ce/H] versus R_{gc} is −0.07 ± 0.05 dex/kpc. A comparison of the slope value provided by the current sample of stars for Ce analysis with the results of previous studies indicates that the data are consistent with the results of the previous study.

In Figure 4 we compare our results with chemical evolution models that investigate F to put constraints on its cosmic origin. The different production channels come from various major sources, such as rotating and nonrotating massive stars, AGB stars, W-R stars, type II supernova, and novae, which are suggested to produce the F that we observe today. Figure 4 shows [F/Fe] and [F/H] against both [Fe/H] and age. We compare the models with the stars from our previous analysis, some literature OCs, and field stars (similar to Fig. 2).

The GCE models utilized for comparison in the current study are the same that were developed for our previous paper, Seshashayana et al. (2024). There are three sets of yields con-

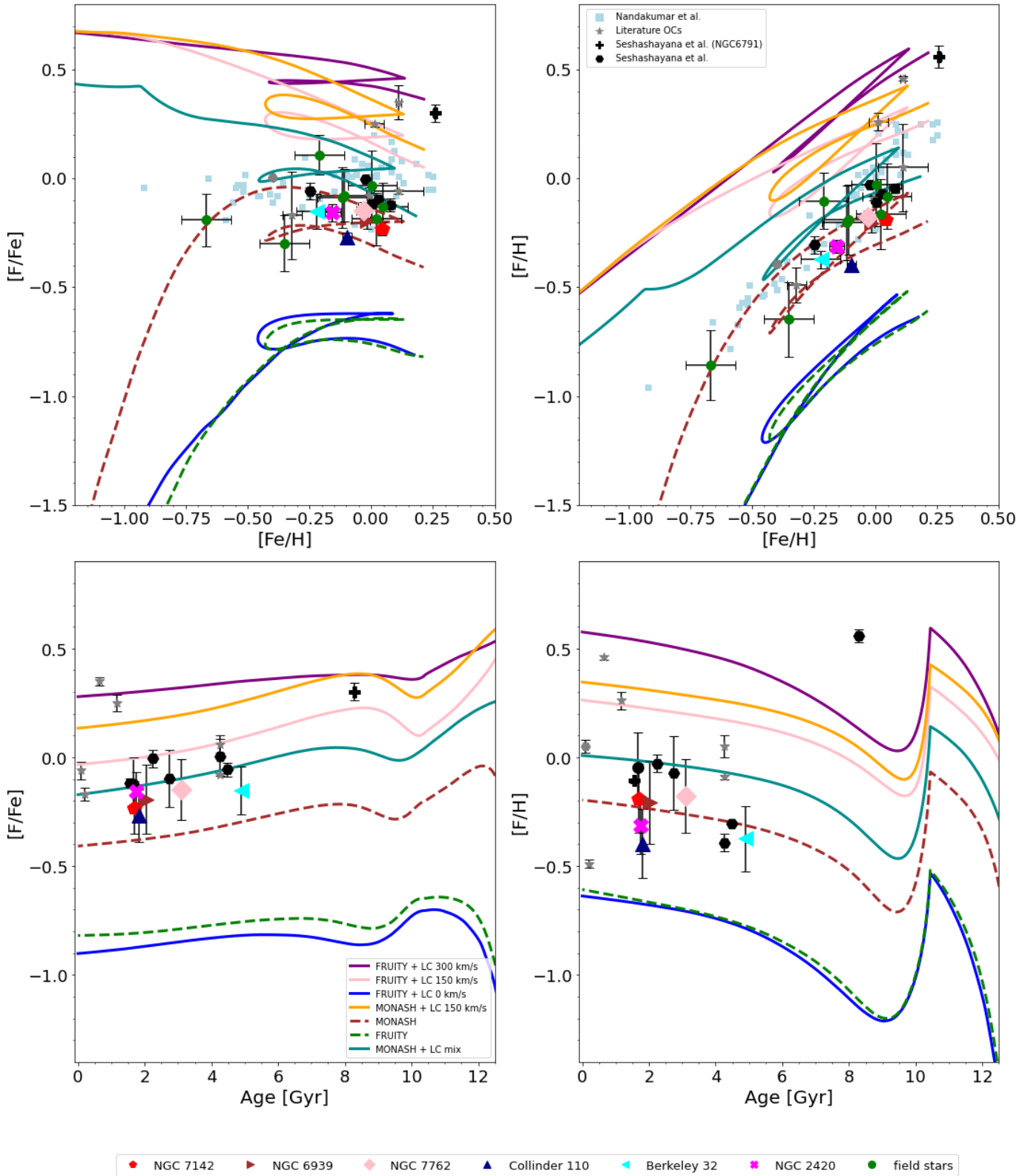

Fig. 4. [F/Fe] and [F/H] against [Fe/H] (top) and age (bottom). The data points are measurements for OCs as well as field stars, and the lines are predicted from theoretical models. The OCs from our previous sample are shown as black hexagons. The figure shows the models that allow F to form from both LIMS and massive stars (solid lines) and the models that only allow F to form from AGB stars (dashed lines).

sidered in this model. The massive star yields (including W-R stars) with different rotation rates are assumed to have no rotation ($v_{\rm rot}$ = 0 km/s) (Limongi & Chieffi 2018), and fast-rotating stars with rotation rates ($v_{\rm rot}$ = 150 and 300 km/s). The yields of low- and intermediate-mass stars (LIMSs), such as AGB stars are taken from either the FUll-Network Repository of Updated Isotopic Tables and Yields (FRUITY) database (Cristallo et al. 2009, 2011, 2015) or the yields by

the MONASH team (Lugaro et al. 2012; Fishlock et al. 2014; Karakas & Lugaro 2016; Karakas et al. 2018). For a detailed description of the yields chosen, please refer to our previous paper, Seshashayana et al. (2024).

Based on the data presented in Figure 4, it is clear that the AGB F yields from MONASH are sufficient to roughly explain the F abundances observed, but massive star yields where F is produced in the hydrostatic burning layers are needed when FRUITY yields are considered. The F yields for rotating massive stars from Limongi & Chieffi (2018) result in excessive production of F. Previous studies (Prantzos et al. 2018; Romano et al. 2019) have shown that the $v_{\rm rot}$ of massive stars must be faster at low metallicities, and vice versa. A new model was introduced in Seshashayana et al. (2024, solid cyan line in Fig. 4). In this model, 80% of low-metallicity massive stars are fast rotators, while the remaining 20% are considered to not rotate. The ratio is the other way around when considering solar and super-solar metallicities. A gradual transition exists between the two ranges. The model where yields from LIMSs (MONASH) and massive stars are mixed like this, is the best fit of the observations within the error range.

5. Summary and conclusions

This paper presents a study of stars in six OCs as well as eight field stars. It also presents their stellar parameter values, metallicities, and fluorine, magnesium, and cerium abundances. The sample is composed of a total of 22 stars, of which 14 stars are located in six OCs. The OCs under consideration are NGC 7142, NGC 6939, NGC 7762, Collinder 110, Berkeley 32, and NGC 2420. The objective of this study was to investigate the cosmic origin of F and Ce by analyzing their trends. We compared the abundances of F and Ce with metallicity for both OCs and field stars, as well as with literature values. The abundances of F and Ce for the OCs were plotted against age and $R_{\rm gc}$ to identify global trends. Our sample shows a flat trend when plotting [F/Fe] against metallicity, age, and $R_{\rm gc}$. On the other hand, a downward trend is observed for [F/H] and [Ce/H] versus age and $R_{\rm gc}$, which is consistent with the expected global Galactic gradient. We compared our results with models that assume different F production channels, including low-mass stars with yields from FRUITY (Cristallo et al. 2009, 2011, 2015) and MONASH (Lugaro et al. 2012; Fishlock et al. 2014; Karakas & Lugaro 2016; Karakas et al. 2018), and rotating massive stars Limongi & Chieffi (2018). The FRUITY-LIMSs underproduce F, indicating the need for another source. The abundances are overestimated by rapidly rotating massive stars. However, the yields from MONASH-LIMSs, provide a reasonable fit to our data. When considering age, though, it is evident that an additional source is still necessary. To better explain the observational results, we considered AGB stars (MONASH yields) and a proportion of fast rotators, which varies as a function of metallicity i.e., there ought to be more fast rotators on average with decreasing metallicity (Prantzos et al. 2018; Romano et al. 2019). Although the models provide a satisfactory explanation for the origin of F, a larger sample with a wider variety of ages and galactocentric distances would be beneficial. In particular, it would be advantageous to include younger and older OCs, thereby expanding the current sample. Nevertheless, it is crucial to acknowledge that the majority of OCs observed are not sufficiently older than those included in our present sample. Moreover, the cool giants necessary for the current analysis are not present in younger OCs. For this reason, it would be beneficial to investigate cool dwarfs in such clusters. Nevertheless, the current results strengthen our previous claim that AGB stars alone cannot account for the production of F. Other sources, such as massive stars with varying rotation rates, must also be involved.

Acknowledgements. S.B.S. acknowledges funding from the Crafoord Foundation. A.B. acknowledges funding from INAF MiniGrant 2022. V.D. acknowledges the financial contribution from PRIN MUR 2022 (code 2022YP5ACE) funded by the European Union – NextGenerationEU.

References

Abdurro'uf, Accetta, K., Aerts, C., et al. 2022, ApJS, 259, 35
Abia, C., Recio-Blanco, A., de Laverny, P., et al. 2009, ApJ, 694, 971
Abia, C., Cunha, K., Cristallo, S., et al. 2010, ApJ, 715, L94
Amarsi, A. M., Lind, K., Asplund, M., Barklem, P. S., & Collet, R. 2016, MNRAS, 463, 1518
Amarsi, A. M., Nordlander, T., Barklem, P. S., et al. 2018, A&A, 615, A139
Amarsi, A. M., Nissen, P. E., & Skúladóttir, Á. 2019, A&A, 630, A104
Asplund, M., Amarsi, A. M., & Grevesse, N. 2021, A&A, 653, A141
Baines, E. K., Thomas Armstrong, J., Clark, J. H., et al. 2021, AJ, 162, 198
Bhowmick, A., Pandey, G., & Lambert, D. L. 2020, JApA, 41, 40
Bragaglia, A., Sestito, P., Villanova, S., et al. 2008, A&A, 480, 79
Busso, M., Gallino, R., & Wasserburg, G. J. 1999, ARA&A, 37, 239
Cantat-Gaudin, T., Anders, F., Castro-Ginard, A., et al. 2020, A&A, 640, A1
Carbajo-Hijarrubia, J., Casamiquela, L., Carrera, R., et al. 2024, A&A, 687, A239
Carraro, G., Semenko, E. A., & Villanova, S. 2016, AJ, 152, 224
Carrera, R., & Pancino, E. 2011, A&A, 535, A30
Carrera, R., Bragaglia, A., Cantat-Gaudin, T., et al. 2019, A&A, 623, A80
Civiš, S., Ferus, M., Chernov, V. E., & Zanozina, E. M. 2013, A&A, 554, A24
Corliss, C. H. 1973, J. Res. Natl. Bur. Stand., 77A, 419
Cosentino, R., Lovis, C., Pepe, F., et al. 2014, SPIE Conf. Ser., 9147, 91478C
Cristallo, S., Straniero, O., Gallino, R., et al. 2009, ApJ, 696, 797
Cristallo, S., Piersanti, L., Straniero, O., et al. 2011, ApJS, 197, 17
Cristallo, S., Straniero, O., Piersanti, L., & Gobrecht, D. 2015, ApJS, 219, 40
Cunha, K., Smith, V. V., Lambert, D. L., & Hinkle, K. H. 2003, AJ, 126, 1305
Cunha, K., Smith, V. V., & Gibson, B. K. 2008, ApJ, 679, L17
Cunha, K., Smith, V. V., Hasselquist, S., et al. 2017, ApJ, 844, 145
Demarque, P., Woo, J.-H., Kim, Y.-C., & Yi, S. K. 2004, ApJS, 155, 667
Donor, J., Frinchaboy, P. M., Cunha, K., et al. 2018, AJ, 156, 142
D'Orazi, V., & Randich, S. 2009, A&A, 501, 553
D'Orazi, V., Lucatello, S., Lugaro, M., et al. 2013, ApJ, 763, 22
D'Orazi, V., Baratella, M., Lugaro, M., Magrini, L., & Pignatari, M. 2022, Universe, 8, 110
Fishlock, C. K., Karakas, A. I., Lugaro, M., & Yong, D. 2014, ApJ, 797, 44
Friel, E. D. 1995, ARA&A, 33, 381
Friel, E. D., Janes, K. A., Tavarez, M., et al. 2002, AJ, 124, 2693
Friel, E. D., Jacobson, H. R., & Pilachowski, C. A. 2010, AJ, 139, 1942
Fu, X., Bragaglia, A., Liu, C., et al. 2022, A&A, 668, A4
Grisoni, V., Romano, D., Spitoni, E., et al. 2020, MNRAS, 498, 1252
Guerço, R., Cunha, K., Smith, V. V., et al. 2019, ApJ, 876, 43
Guerço, R., Ramírez, S., Cunha, K., et al. 2022, ApJ, 929, 24
Gustafsson, B., Edvardsson, B., Eriksson, K., et al. 2008, A&A, 486, 951
Holanda, N., Roriz, M. P., Drake, N. A., et al. 2024, MNRAS, 527, 1389
Jacobson, H. R., Friel, E. D., & Pilachowski, C. A. 2007, AJ, 134, 1216
Jacobson, H. R., Pilachowski, C. A., & Friel, E. D. 2011, AJ, 142, 59
Janes, K. A. 1979, ApJS, 39, 135
Jönsson, H., Ryde, N., Harper, G. M., et al. 2014a, A&A, 564, A122
Jönsson, H., Ryde, N., Harper, G. M., Richter, M. J., & Hinkle, K. H. 2014b, ApJ, 789, L41
Jönsson, H., Ryde, N., Spitoni, E., et al. 2017, ApJ, 835, 50
Jorissen, A., Smith, V. V., & Lambert, D. L. 1992, A&A, 261, 164
José, J., & Hernanz, M. 1998, AIP Conf. Ser., 425, 539
Karakas, A. I., & Lugaro, M. 2016, ApJ, 825, 26
Karakas, A. I., Lugaro, M., Carlos, M., et al. 2018, MNRAS, 477, 421
Kobayashi, C., Izutani, N., Karakas, A. I., et al. 2011a, ApJ, 739, L57
Kobayashi, C., Karakas, A. I., & Umeda, H. 2011b, MNRAS, 414, 3231
Kupka, F., Piskunov, N., Ryabchikova, T. A., Stempels, H. C., & Weiss, W. W. 1999, A&AS, 138, 119
Kupka, F. G., Ryabchikova, T. A., Piskunov, N. E., Stempels, H. C., & Weiss, W. W. 2000, Balt. Astron., 9, 590
Lada, C. J., & Lada, E. A. 2003, ARA&A, 41, 57
Lauer, A., Chatzopoulos, E., Clayton, G. C., Frank, J., & Marcello, D. C. 2019, MNRAS, 488, 438
Limongi, M., & Chieffi, A. 2018, ApJS, 237, 13

Lucatello, S., Masseron, T., Johnson, J. A., Pignatari, M., & Herwig, F. 2011, ApJ, 729, 40
Lugaro, M., Karakas, A. I., Stancliffe, R. J., & Rijs, C. 2012, ApJ, 747, 2
Magrini, L., Randich, S., Kordopatis, G., et al. 2017, A&A, 603, A2
Magrini, L., Viscasillas Vázquez, C., Spina, L., et al. 2023, A&A, 669, A119
Maiorca, E., Randich, S., Busso, M., Magrini, L., & Palmerini, S. 2011, ApJ, 736, 120
Maiorca, E., Uitenbroek, H., Uttenthaler, S., et al. 2014, ApJ, 788, 149
Menon, A., Herwig, F., Denissenkov, P. A., et al. 2013, ApJ, 772, 59
Menon, A., Karakas, A. I., Lugaro, M., Doherty, C. L., & Ritter, C. 2019, MNRAS, 482, 2320
Meynet, G., & Arnould, M. 2000, A&A, 355, 176
Mishenina, T., Pignatari, M., Carraro, G., et al. 2015, MNRAS, 446, 3651
Montelius, M., Forsberg, R., Ryde, N., et al. 2022, A&A, 665, A135
Myers, N., Donor, J., Spoo, T., et al. 2022, AJ, 164, 85
Nandakumar, G., Ryde, N., Casagrande, L., & Mace, G. 2023a, A&A, 675, A23
Nandakumar, G., Ryde, N., & Mace, G. 2023b, A&A, 676, A79
Nault, K. A., & Pilachowski, C. A. 2013, AJ, 146, 153
Oliva, E., Biliotti, V., Baffa, C., et al. 2012a, SPIE Conf. Ser., 8453, 84532T
Oliva, E., Origlia, L., Maiolino, R., et al. 2012b, SPIE Conf. Ser., 8446, 84463T
Origlia, L., Oliva, E., Baffa, C., et al. 2014, SPIE Conf. Ser., 9147, 91471E
Overbeek, J. C., Friel, E. D., & Jacobson, H. R. 2016, ApJ, 824, 75
Pancino, E., Carrera, R., Rossetti, E., & Gallart, C. 2010, A&A, 511, A56
Pancino, E., Lardo, C., Altavilla, G., et al. 2017, A&A, 598, A5
Pandey, G. 2006, ApJ, 648, L143
Pandey, G., Lambert, D. L., & Kameswara Rao, N. 2008, ApJ, 674, 1068
Pilachowski, C. A., & Pace, C. 2015, AJ, 150, 66
Piskunov, N., & Valenti, J. A. 2017, A&A, 597, A16
Piskunov, N. E., Kupka, F., Ryabchikova, T. A., Weiss, W. W., & Jeffery, C. S. 1995, A&AS, 112, 525
Prantzos, N., Abia, C., Limongi, M., Chieffi, A., & Cristallo, S. 2018, MNRAS, 476, 3432
Rainer, M., Harutyunyan, A., Carleo, I., et al. 2018, SPIE Conf. Ser., 10702, 1070266
Randich, S., Gilmore, G., Magrini, L., et al. 2022, A&A, 666, A121
Recio-Blanco, A., de Laverny, P., Worley, C., et al. 2012, A&A, 538, A117
Romano, D., Matteucci, F., Zhang, Z.-Y., Ivison, R. J., & Ventura, P. 2019, MNRAS, 490, 2838
Romano, D., Magrini, L., Randich, S., et al. 2021, A&A, 653, A72
Ryde, N., Hartman, H., Oliva, E., et al. 2019, A&A, 631, L3
Ryde, N., Jönsson, H., Mace, G., et al. 2020, ApJ, 893, 37
Sauval, A. J., & Tatum, J. B. 1984, ApJS, 56, 193
Schuler, S. C., Cunha, K., Smith, V. V., et al. 2007, ApJ, 667, L81
Seshashayana, S. B., Jönsson, H., D'Orazi, V., et al. 2024, A&A, 683, A218
Sestito, P., Bragaglia, A., Randich, S., et al. 2006, A&A, 458, 121
Spina, L., Ting, Y. S., De Silva, G. M., et al. 2021, MNRAS, 503, 3279
Spina, L., Magrini, L., & Cunha, K. 2022, Universe, 8, 87
Spitoni, E., Matteucci, F., Jönsson, H., Ryde, N., & Romano, D. 2018, A&A, 612, A16
Timmes, F. X., Woosley, S. E., & Weaver, T. A. 1995, AIP Conf. Ser., 327, 543
Valenti, J. A., & Piskunov, N. 1996, A&AS, 118, 595
Viscasillas Vázquez, C., Magrini, L., Casali, G., et al. 2022, A&A, 660, A135
Wehrhahn, A., Piskunov, N., & Ryabchikova, T. 2023, A&A, 671, A171
Werner, K., Rauch, T., & Kruk, J. W. 2005, A&A, 433, 641
Woosley, S. E., & Haxton, W. C. 1988, Nature, 334, 45
Yong, D., Carney, B. W., & Friel, E. D. 2012, AJ, 144, 95
Zhang, Y., & Liu, X. W. 2005, ApJ, 631, L61
Zhong, J., Chen, L., Wu, D., et al. 2020, A&A, 640, A127